Pseudo-Adiabatic Operation and Runaway in Tubular Reactors

Hua Wu
Ausimont Research and Development Center, Montedison, 20021 Bollate (Milano), Italy

Massimo Morbidelli
Chemical Engineering Dept./LTC, ETH Zentrum, Universitatstrasse 6, CH-8092 Zurich, Switzerland

Arvind Varma
Dept. of Chemical Engineering, University of Notre Dame, Notre Dame, IN 46556

Critical conditions for thermal runaway in homogeneous tubular reactors with either constant or cocurrent external cooling were investigated through the applications of the generalized sensitivity criterion using reactor axial coordinate as the independent variable, and compared with those predicted by geometry-based criteria. All criteria are found to provide rather similar results when a hot spot is present inside the reactor. When the hot spot shifts to the reactor outlet, leading to the so-called pseudo-adiabatic operation (PAO), the geometry-based criteria become either invalid or conservative with respect to the generalized one. In addition, when the generalized criterion is applied to the cases where the PAO is present, it is required to use the axial coordinate rather than reactant conversion as the independent variable to predict the critical conditions, and the obtained runaway boundaries in the reactor parameter plane coincide with the PAO boundaries.

Introduction

For exothermic reactions occurring in a tubular reactor, a temperature peak or hot spot is usually exhibited at some location along the reactor length. This hot spot should be bounded within specific limits, because it may seriously affect reactor safety and performance. The magnitude of the hot spot depends on the system parameters such as operating conditions, physicochemical properties, and reaction kinetics. For specific values of the operating conditions, the hot spot may undergo large variations in response to relatively small changes in the operating conditions or parameters. In this case, the reactor is said to operate in the runaway or parametrically sensitive region. In practical applications, it is clearly desired to avoid this operation region in the earlier stages of reactor design. This motivated the development of various *a-priori* criteria (Barkelew, 1959; Thomas, 1961; Adler and Enig, 1964; Dente and Collina, 1964; Hlavacek et al., 1969; van Welsenaere and Froment, 1970; Morbidelli and Varma, 1982; Henning and Perez, 1986; Hagan et al., 1988) that distinguish the safe from the runaway operation regions in the system parameter space.

Most of the criteria reported in the literature are based on the temperature behavior in the temperature-conversion phase plane. In other words, in the reactor model, instead of the axial coordinate, reactant conversion has been used as the independent variable. This implicitly assumes that a temperature maximum (hot spot) is always present in the reactor. Indeed, in the case of batch reactors, this is a safe approach, since as time passes by conversion increases from 0 to 1, and in the typical case where the coolant temperatures does not exceed the initial temperature, a temperature maximum is always reached. For tubular reactors, such an approach ignores the constraint imposed on the system behavior by the finite reactor length that limits conversion. As shown by Soria Lopez et al. (1981) in the case of cocurrent external cooling, operations without a hot spot (that is, where the temperature along the reactor axis increases monotonically) can oc-

Correspondence concerning this article should be addressed to A. Varma.

cur under certain conditions. These are referred to as *pseudo-adiabatic operations* (PAO). In order to account for this kind of operation in the investigations of reactor sensitivity behavior, the criteria previously developed have to be properly modified. This is the purpose of the present work.

After having derived the basic model equations, we identify, in the section on pseudo-adiabatic operation, the PAO region in various parameter phase planes for both constant and cocurrent external cooling. We analyze the influence of PAO on the reactor runaway regions predicted by the Morbidelli and Varma (1988) generalized and various geometry-based criteria. It will be seen that most of these criteria provide similar results when the hot spot is present inside the reactor. When the hot spot shifts to the reactor outlet, leading to PAO, however, the runaway regions predicted by all criteria deviate from one another. In this case, the best representation of the reactor runaway behavior is given by the generalized criterion using axial coordinate as the independent variable, and the obtained runaway boundaries coincide with the PAO boundaries.

Basic Equations

Consider a tubular plug-flow reactor with cocurrent external cooling, where an exothermic, nth order reaction occurs. The steady-state mass and energy balances are represented by the following equations

$$\frac{dC}{dl} = -\frac{\rho_B}{\nu^o}\cdot k(T)\cdot C^n \tag{1}$$

$$\frac{dT}{dl} = \frac{(-\Delta H)}{\rho\cdot c_p}\cdot\frac{\rho_B}{\nu^o}\cdot k(T)\cdot C^n - \frac{4U}{d_t\cdot\nu^o\cdot\rho\cdot c_p}\cdot(T-T_{co}) \tag{2}$$

$$\frac{dT_{co}}{dl} = \frac{\pi\cdot d_t\cdot t_n\cdot U}{c_{p,co}\cdot w_{co}}\cdot(T-T_{co}) \tag{3}$$

with the inlet conditions (ICs)

$$C = C^i, \quad T = T^i \quad \text{and} \quad T_{co} = T_{co}^i \quad \text{at} \quad l = 0 \tag{4}$$

By introducing the following dimensionless variables

$$x = \frac{C^i - C}{C^i}; \quad \theta = \frac{T - T^i}{T^i}\cdot\gamma; \quad \theta_{co} = \frac{T_{co} - T^i}{T^i}\cdot\gamma; \quad z = \frac{l}{L} \tag{5}$$

and dimensionless parameters

$$Da = \frac{\rho_B\cdot k(T^i)\cdot(C^i)^{n-1}\cdot L}{\nu^o}; \quad B = \frac{(-\Delta H)\cdot C^i}{\rho\cdot c_p\cdot T^i}\cdot\gamma;$$

$$\gamma = \frac{E}{R_g\cdot T^i}; \quad St = \frac{4\cdot U\cdot L}{d_t\cdot\nu^o\cdot\rho\cdot c_p}; \quad \tau = \frac{\pi\cdot d_t^2\cdot t_n\cdot\nu^o\cdot\rho\cdot c_p}{4\cdot c_{p,co}\cdot w_{co}} \tag{6}$$

we may write Eqs. 1 to 4 in dimensionless form

$$\frac{dx}{dz} = Da\cdot\exp\left(\frac{\theta}{1+\theta/\gamma}\right)\cdot(1-x)^n = f_1(x,\theta,\underline{\phi}) \tag{7}$$

$$\frac{d\theta}{dz} = Da\cdot B\cdot\exp\left(\frac{\theta}{1+\theta/\gamma}\right)\cdot(1-x)^n - St\cdot(\theta-\theta_{co}) = f_2(x,\theta,\underline{\phi}) \tag{8}$$

$$\frac{d\theta_{co}}{dz} = \tau\cdot St\cdot(\theta-\theta_{co}) \tag{9}$$

$$x = 0, \quad \theta = \theta^i \quad \text{and} \quad \theta_{co} = \theta_{co}^i \quad \text{at} \quad z = 0 \tag{10}$$

where $\underline{\phi}$ indicates the vector of all the input parameters present in the model. From the above equations, an algebraic relation between reactor temperature, coolant temperature, and conversion can be readily established. Substituting Eqs. 7 and 9 into Eq. 8 leads to

$$\frac{d\theta}{dz} = B\cdot\frac{dx}{dz} - \frac{1}{\tau}\cdot\frac{d\theta_{co}}{dz} \tag{11}$$

which, when integrated with the ICs (Eq. 10), gives

$$\theta_{co} = \theta_{co}^i + [B\cdot x - (\theta-\theta^i)]\cdot\frac{1}{\tau} \tag{12}$$

This indicates that the coolant temperature θ_{co} can be readily computed at any location along the reactor, once the values of conversion x and reactor temperature θ are known. Thus, a complete description of the system is obtained by using only two differential equations, Eqs. 7 and 8, where the coolant temperature is given by Eq. 12.

It is worth noting that the parameter τ represents the heat capacity ratio between the reaction mixture and the external coolant. Thus, for very small values of τ, the classical case of external coolant at constant temperature is obtained, as it clearly appears from Eq. 12 where as $\tau \to 0$ we have $\theta_{co} = \theta_{co}^i$. This is typically the case when the coolant undergoes a phase transition.

Pseudo-Adiabatic Operation

When taking conversion rather than axial coordinate as the independent variable, that is, dividing Eq. 8 by Eq. 7, we reduce the model to a single equation

$$\frac{1}{B}\cdot\frac{d\theta}{dx} = 1 - \frac{St}{B\cdot Da}\cdot\frac{\theta-\theta_{co}}{(1-x)^n}\cdot\exp\left(-\frac{\theta}{1+\theta/\gamma}\right) \tag{13}$$

with the inlet condition

$$\theta = \theta^i \quad \text{at} \quad x = 0 \tag{14}$$

where θ_{co} is constant for constant external cooling, and in practice $\theta_{co} \le \theta^i$ for exothermic reactions. It is seen from Eqs. 13 and 14 that for positive order kinetics $(d\theta/dx) < 0$ as $x \to 1$,

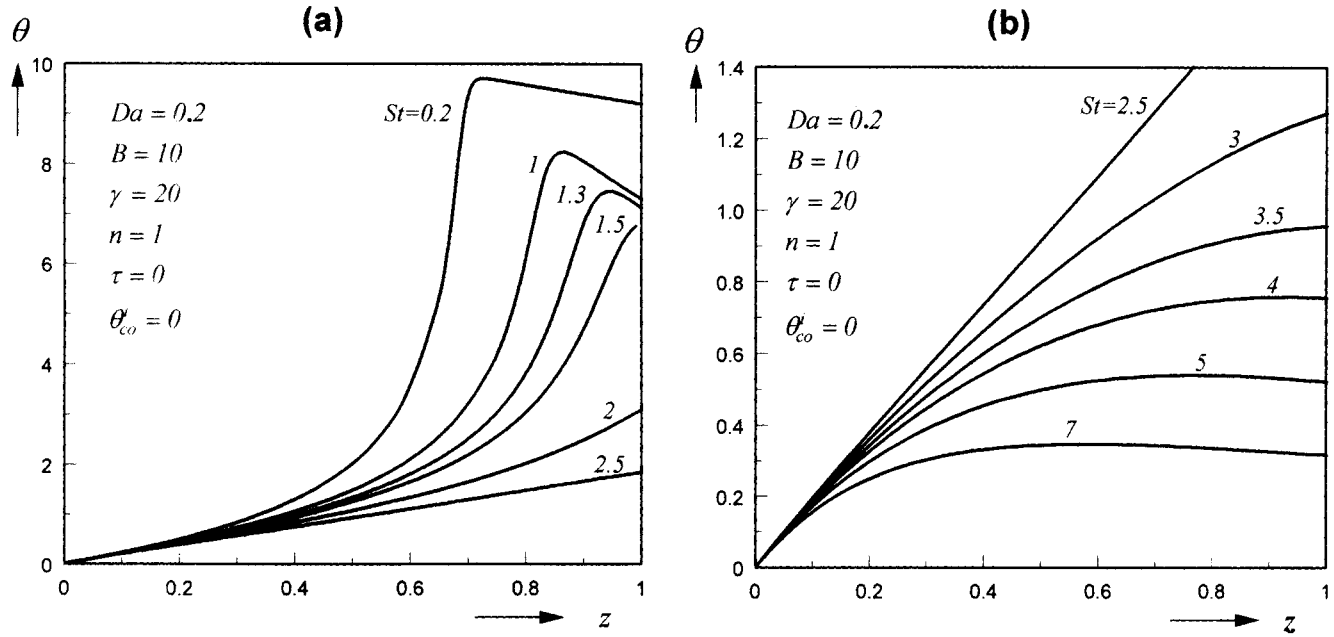

Figure 1. Temperature profiles along the reactor axis for various values of *St*, indicating the occurrence of the PAO region.

indicating the occurrence of a maximum in the temperature vs. conversion profile. Thus, when conversion is taken as the independent variable, PAO does not occur. Moreover, with this approach the temperature and conversion vs. reactor length behavior is obviously lost.

On the other hand, when the axial coordinate is taken as the independent variable (Eqs. 7, 8, 10 and 12), the PAO can indeed occur in the case of constant external cooling. This is illustrated in Figure 1 where, fixed values of B and all the other parameters, the temperature profiles as a function of the axial coordinate are shown for various values of St. The corresponding conversion values are shown in Figure 2. In particular, in Figure 1a it can be seen that for $St = 0.2$, the hot spot is located at about $z = 0.72$, and the corresponding temperature value is very high. In this case, conversion is practically complete right after the hot spot, as shown in Figure 2a. Thus, the occurrence of a maximum in the temperature profile, which in the following will be referred to as *hot*

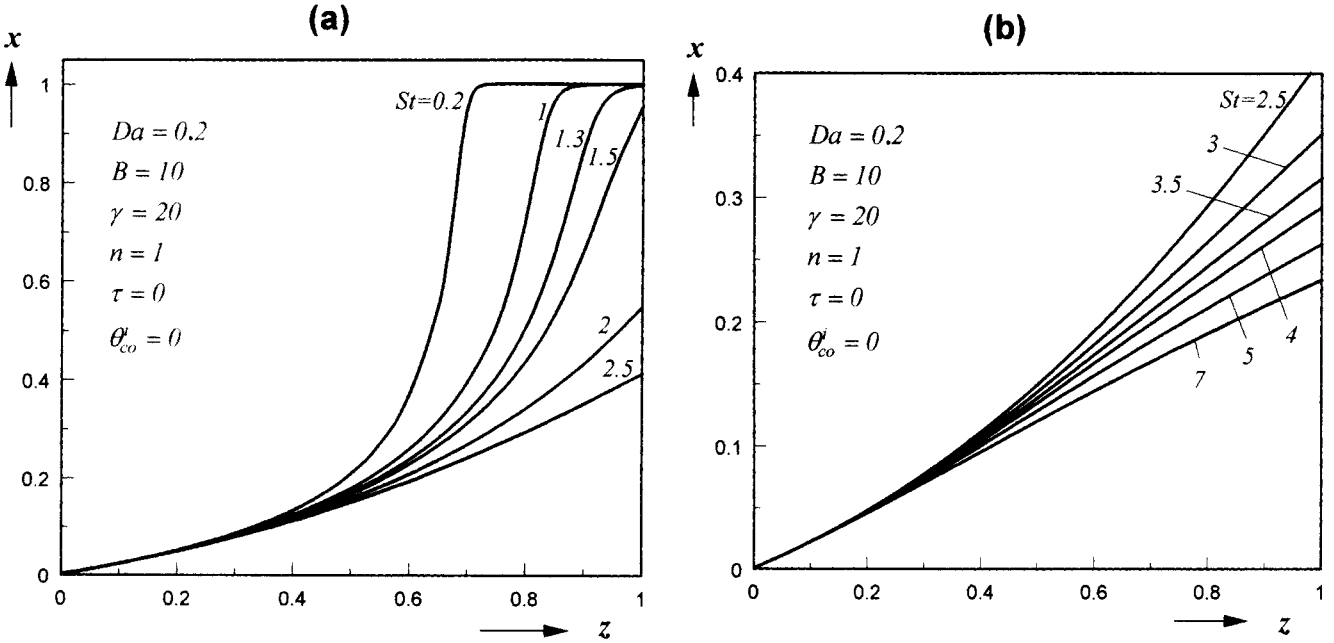

Figure 2. Profiles of the reactant conversion along the reactor axis for various values of *St*, corresponding to the conditions in Figure 1.

spot operation (HSO), is due to the complete conversion of the reactant. In the portion of the reactor following the hot spot, the heat generation is in fact negligible while heat removal is continuing, thus leading to a temperature decrease. Let us now increase, say, the wall heat-transfer coefficient, which corresponds to larger values of St. Since the temperature values along the reactor decrease, leading to lower reaction rates, a longer portion of the reactor is required to complete the reaction, and the hot spot moves toward the reactor outlet. When the St value increases further, a critical value is reached (1.48 in Figure 1a) where the hot spot is washed out from the reactor and PAO is obtained. It is worth noting that in the PAO region, not only the temperature values in the reactor decrease as St increases, but also the shape of the temperature profile changes from concave (such as $St = 2$ and 2.5 in Figure 1a) to convex (such as $St = 3$ and 3.5 in Figure 1b), so that when St increases further, a second critical value is reached, that is, 3.66 in Figure 1b, where a maximum appears again in the reactor temperature profile. However, in this region of reactor operating conditions, both the temperature value at the hot spot and the conversion at the reactor outlet are very low. Thus, this region of the HSO is characterized by a very low reaction rate in the reactor, and the occurrence of a temperature maximum is due to the heat removal rate overtaking the rate of heat generation even before significant reactant depletion. This situation is clearly far away from reactor temperature runaway conditions.

PAO region in the case of constant coolant temperature

In the example discussed above, we have seen that by increasing the Stanton number, the system undergoes two transitions in the operation region, going from HSO to PAO and then back to HSO. By repeating this exercise for various values of the dimensionless heat of reaction parameter B, we can identify a region of PAO in the $St - B$ parameter plane. Some of these are shown in Figure 3 corresponding to various values of the Damköhler number Da. The boundaries of these regions were obtained by numerically integrating Eqs. 7 and 8 with Eqs. 10 and 12, and using a trial-and-error procedure to find the conditions leading to $d\theta/dz = 0$ at the reactor outlet. It appears that the PAO region is generally enclosed by a boundary formed by lower and upper branches. As discussed above in the context of Figures 1 and 2, the HSO region to the right of the lower branch is characterized by high reaction rates, thus substantially leading to complete outlet conversion. On the other hand, the HSO region above the upper branch is characterized by low reaction rates, and, hence, low outlet conversion. In Figure 3, it can be seen that the PAO region shrinks as Da increases. This occurs because increasing Da value implies the increase of either the reactor length or the reaction rate, which both favor the appearance of a hot spot along the reactor. Moreover, the existence of two distinct branches of the boundaries of the PAO region tends to disappear at high Da values, as is for example the case for $Da = 1$ in Figure 3.

The PAO regions are also shown in the $St - Da$ parameter plane in Figure 4 for various values of the dimensionless activation energy γ. Larger γ values lead to higher acceleration of the reaction rate in response to an increase of the system temperature, thus requiring a shorter reactor for completing

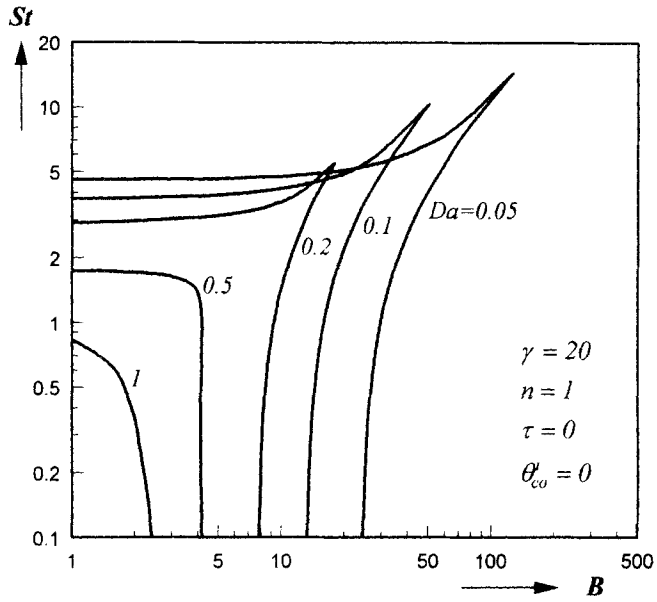

Figure 3. PAO regions in the St-B parameter plane for various values of Da.

Case with the external coolant at a constant temperature.

the reaction. For this, the lower branch of the PAO boundary moves towards the region of lower Da values as γ increases. On the other hand, the influence of γ on the upper branch is very limited. This is because around the upper branch the temperature in the entire reactor is very low and slightly higher than the inlet temperature. In this case, variations in γ do not change significantly the reaction rate. Finally, note

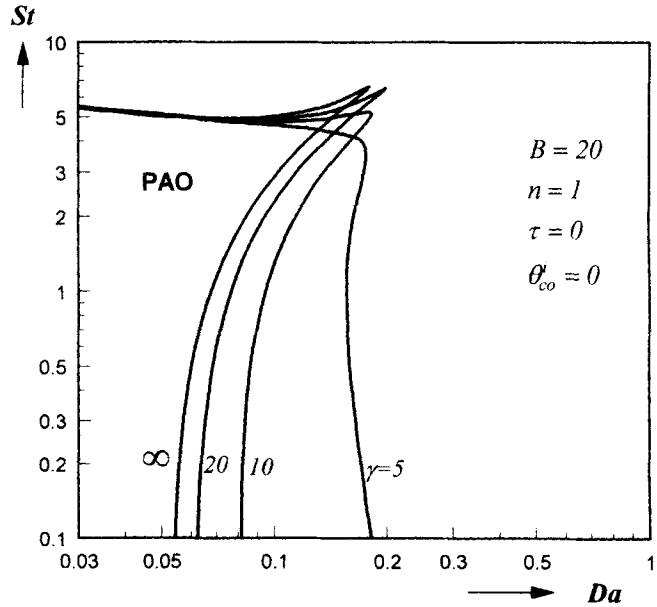

Figure 4. PAO regions in the St-Da parameter plane for various values of the dimensionless activation energy γ.

Case with the external coolant at a constant temperature.

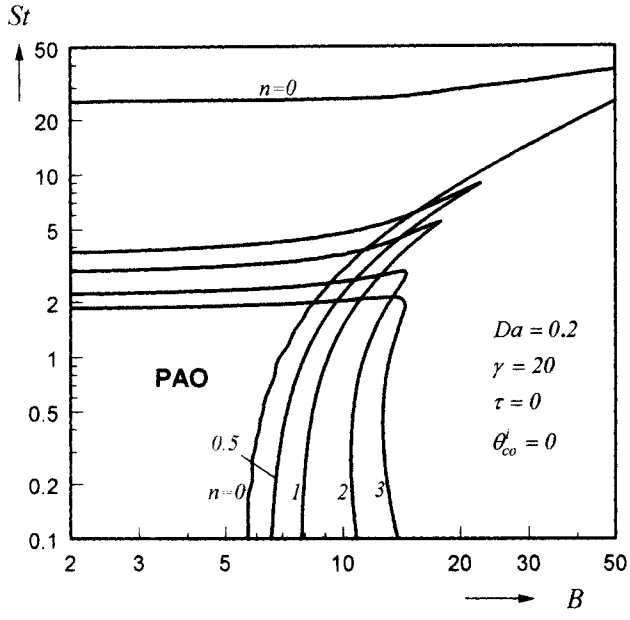

Figure 5. PAO regions in the $St - B$ parameter plane for various values of the reaction order n.

Case with the external coolant at a constant temperature.

that γ has an asymptotic effect on the system behavior. For the case shown in Figure 4, when γ values are higher than 40, the influence of γ on the PAO region becomes negligible.

The influence of the reaction order n on the PAO region is shown in Figure 5. As n increases, the lower branch of the PAO boundary moves towards higher B values. This behavior can be explained by considering that a higher reaction rate is obtained with a lower value of reaction order. The occurrence of the hot spot in the region to the right of the lower branch, as discussed earlier, is due to essentially complete reactant conversion before the reactor outlet. Then, for a reaction with lower n, due to the higher reaction rate, the hot spot appears for a lower value of the heat of reaction (that is, at a lower B value) and, therefore, the lower branch moves towards lower B values. In the same figure, it is seen that the upper branch of the PAO boundary moves towards lower St values as n increases. This arises because in the region above the upper branch, the occurrence of the hot spot is due to the heat removal rate overtaking the heat generation rate. Then, since a higher reaction order leads to a lower reaction rate and consequently to a lower heat generation rate, the hot spot occurs at a lower heat removal rate (that is, a lower St).

The PAO boundary in the case of a zeroth order reaction is also shown in Figure 5. Again, the HSO region over the upper branch is characterized by a very low reaction rate in the reactor, and the occurrence of a temperature maximum is due to the heat removal rate overtaking the rate of heat generation even before significant reactant depletion. Note that for the zeroth order reaction, the temperature profile along the reactor axis undergoes discontinuity when conversion is complete, since the reaction rate drops from a finite value to zero. In this case, the condition for determining the lower branch of the PAO boundary is complete conversion at reactor outlet, that is, $x = 1$ at $z = 1$.

PAO region in case of varying coolant temperature

The case of external coolant at constant temperature considered in the previous section corresponds to $\tau = 0$ in Eq. 12, which implies an extremely large heat capacity $c_{p,co}$ or an extremely large coolant flow rate w_{co}. This condition is easily achieved at the laboratory scale, but is difficult at the industrial scale, where in general $\tau > 0$. Let us consider the case of a first-order reaction with $\gamma = 20$ and $Da = 0.2$, whose PAO region in the $St - B$ parameter plane was shown previously in Figure 3 for constant external cooling, that is, $\tau = 0$. This has been reproduced in Figure 6 and compared with the PAO regions computed for various values of $\tau > 0$. It is seen that the upper branch of the PAO boundary exists only for very small τ values, that is, $\tau < 0.04$ in this case. For $\tau \geq 0.05$, a different shape for the PAO regions is found involving only one transition between PAO and HSO. The transition between these two different shapes of the PAO regions occurs through rather peculiar intermediate shapes such as the one shown in Figure 6b for $\tau = 0.04$, where a HSO penisula is located inside the PAO region. This can also take the form of an HSO island, as will be discussed later in the context of Figure 12b.

On physical grounds, this can be explained by considering that, as discussed in the previous section, the HSO region located above the upper branch of the PAO region for $\tau = 0$ is characterized by low reaction rates and relatively low outlet conversion. This is due to the strong heat removal rate (large St), which cools down the reacting mixture even before significant reactant conversion can occur. For $\tau > 0$, since the coolant temperature increases along the reactor axis, the driving force for heat removal is reduced, and, consequently, the internal temperature increases, leading to larger reaction rates. Accordingly, a PAO rather than a HSO is developed for the reactor. In other words, for the same PAO to HSO transition to occur, the decrease in the temperature driving force arising when $\tau > 0$ requires larger St values than those observed at $\tau = 0$. Therefore, the upper branch of the PAO boundary moves upwards as τ increases.

It is worth mentioning the explicit expression, derived by Soria Lopez et al. (1981), to predict the PAO boundary for a first-order reaction, which in our notation becomes

$$\frac{\tau \cdot St}{Da} = \exp\left(\frac{\theta_\infty}{1 + \theta_\infty/\gamma}\right) \tag{15}$$

where θ_∞ is defined as the limiting reactor temperature for PAO (that is, the temperature maximum corresponding to the PAO boundary) and is given by

$$\theta_\infty = \frac{\theta^i_{co} + (B + \theta^i)\cdot\tau}{1 + \tau} \tag{16}$$

The derivation of this expression is based on the consideration that at the PAO boundary, the internal temperature maximum is located at the reactor outlet, where it is assumed that conversion is complete and reactor and coolant temperatures are equal. Of course, this approximation is less accurate for slow reaction rate, that is, small Da, and sufficiently low coolant heat capacity, that is, large τ. This is confirmed by

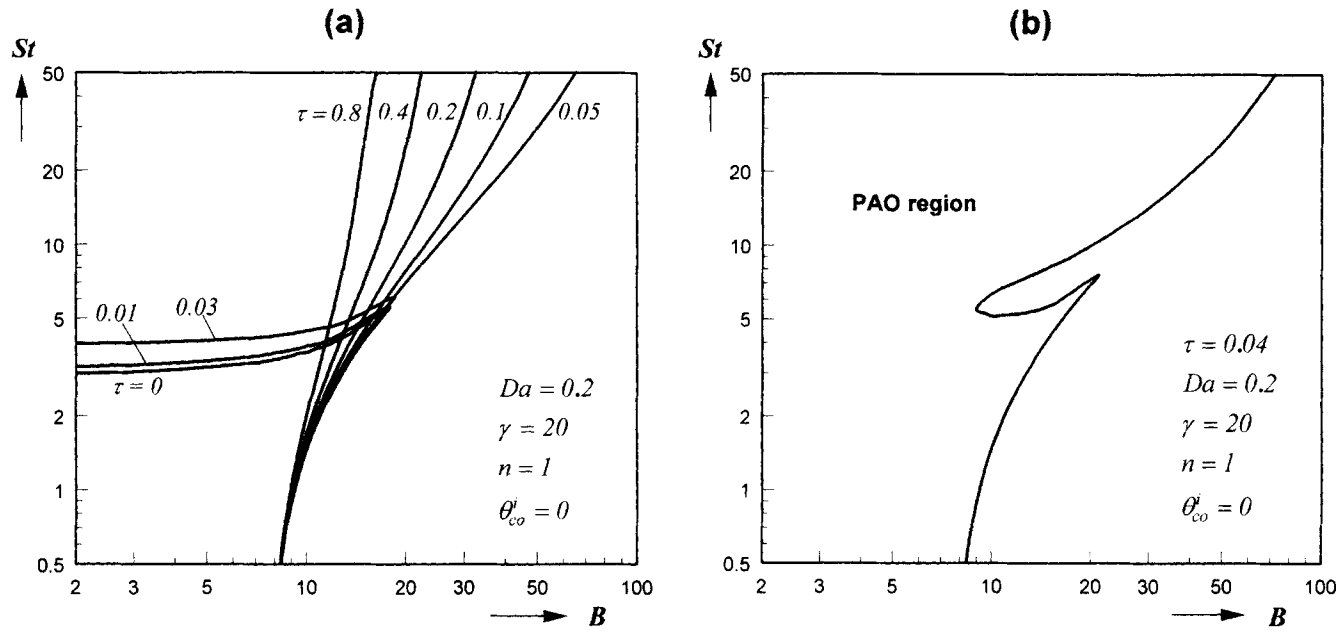

Figure 6. Influence of the cocurrent external cooling (τ) on the PAO region in the $St - B$ parameter plane.

the comparison between the PAO regions calculated by Eq. 15 and those computed numerically in the $\tau - B$ parameter plane shown in Figure 7 for various values of Da. It is seen that for large Da values, the explicit expression (Eq. 15) indeed provides satisfactory results for a rather wide range of τ values. On the other hand, for lower Da values, the predicted boundaries are accurate only at low τ values.

It is worth noting that, similarly to the $St - B$ parameter plane shown in Figure 3, the PAO boundaries in the $\tau - B$ parameter plane exhibit two branches (lower and upper) with respect to B. However, in this case the HSO region below the lower branch is characterized by low reaction rates and relatively low outlet conversion, while the HSO region above the upper branch is characterized by high reaction rates and essentially complete outlet conversion.

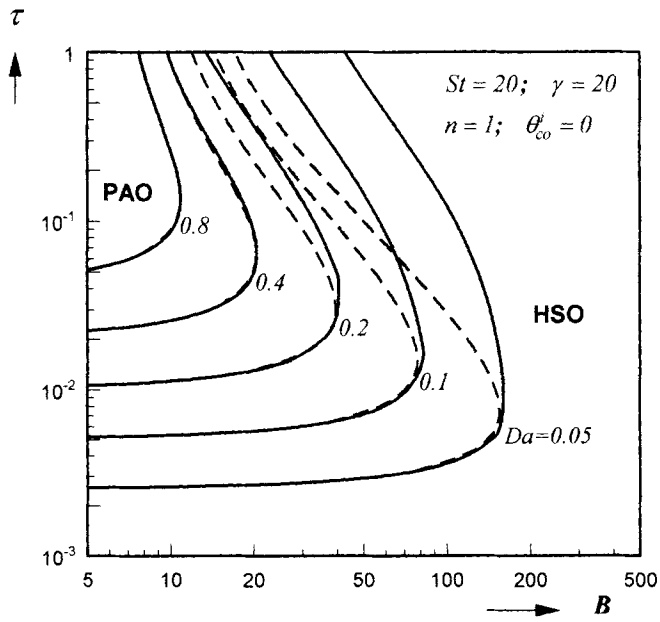

Figure 7. PAO boundaries in the $\tau - B$ parameter plane, calculated numerically (solid curves) and predicted by the explicit expression derived by Soria Lopez et al. (1981) (broken curves) for various values of Da.

Influence of PAO on Runaway Regions

The influence of the PAO on the runaway region can be investigated using Morbidelli and Varma (1988) generalized criterion. We consider the temperature maximum θ^* along the reactor as the objective. Thus, the normalized objective sensitivity is defined by

$$S(\theta^*;\phi) = \frac{\phi}{\theta^*}\cdot\left(\frac{\partial\theta^*}{\partial\phi}\right) = \frac{\phi}{\theta^*}\cdot s(\theta^*;\phi) \qquad (17)$$

where ϕ is one of the independent model parameters, and the objective sensitivity $s(\theta^*;\phi)$ corresponds to the local sensitivity $s(\theta;\phi)$ at the hot spot ($\theta = \theta^*$). The criticality for runaway is defined as the situation where the value of the normalized objective sensitivity $S(\theta^*;\phi)$ is maximum or minimum. Note that, when the reactor operates in the PAO region with no maximum in the temperature profile along the reactor, then θ^* is taken as the temperature value at the reactor outlet.

The objective sensitivity $s(\theta^*;\phi)$ has been computed by the direct differential method, that is, by integrating the following sensitivity equations

$$\frac{ds(x;\phi)}{dz} = \frac{\partial f_1}{\partial x}\cdot s(x;\phi) + \frac{\partial f_1}{\partial\theta}\cdot s(\theta;\phi) + \frac{\partial f_1}{\partial\phi} \qquad (18)$$

$$\frac{ds(\theta;\phi)}{dz} = \frac{\partial f_2}{\partial x}\cdot s(x;\phi) + \frac{\partial f_2}{\partial\theta}\cdot s(\theta;\phi) + \frac{\partial f_2}{\partial\phi} \qquad (19)$$

with ICs

$$s(x;\phi)=0 \quad \text{and} \quad s(\theta;\phi)=\delta(\phi-\theta^i) \quad \text{at} \quad z=0 \tag{20}$$

together with the system Eqs. 7, 8, 10 and 12. The above equations are obtained by differentiating Eqs. 7, 8 and 10 with respect to ϕ. The value of the normalized objective sensitivity $S(\theta^*;\phi)$ is computed from Eq. 17 using the value of $s(\theta;\phi)$ at $\theta=\theta^*$.

In the following, we compare the regions corresponding to PAO with the regions corresponding to runaway predicted by the MV (MV = Morbidelli and Varma, 1988) generalized criterion using axial coordinate (that is, z-MV) or reactant conversion (that is, x-MV) as the independent variable.

Runaway region with constant coolant temperature

Let us first consider as an example the case of a first-order reaction with $Da=0.1$ and $\gamma=20$. The pseudo-adiabatic operation occurs in a large portion of the $St-B$ parameter plane, as shown in Figure 8, where curve 2, composed of two branches, represents the boundary of the PAO region. In the same figure the critical conditions for runaway are also reported as computed using various criteria. Curves 1 and 3 are the critical conditions predicted by the z-MV and x-MV criteria, respectively. Curves 4, 5, 6 and 7 are the results given respectively by the DC (Dente and Collina, 1964), HP (Henning and Perez, 1986), AE (Adler and Enig, 1964) and VF (van Welsenaere and Froment, 1970) criteria. It is seen that when the reactor operates in the HSO region (that is, to the right of the point indicated with the symbol ●), all criteria predict substantially the same critical conditions for runaway. When the reactor operates in the PAO region, however, the predictions of all criteria deviate from one another. Moreover, the boundaries of the runaway region predicted by the z-MV criterion in this case are coincident with the lower branch of the PAO boundary, while those predicted by all the other criteria fall inside the PAO region.

Let us first discuss the differences in the predictions of the z-MV and x-MV criteria in the PAO region. For example, for $B=20$ in Figure 8, the critical St values predicted by the z-MV and x-MV criteria are 2.31 and 3.25, respectively. Note that under these conditions, both critical values exhibit the generalized feature, as shown in Figures 9 and 10, where it can be seen that in both cases the normalized objective sensitivities to five different parameters (B, Da, St, γ and n) reach a maximum or a minimum at the same value of St. Thus, the difference in the predictions of the two criteria is not due to an intrinsically insensitive behavior of the system in this region. The reason is the occurrence of the PAO region for the reactor. The z-MV criterion, by taking the axial coordinate as the independent variable, can properly account for this behavior. In particular, it can resolve that the reactor is too short for developing a local temperature maximum, so that the temperature profile is monotonically increasing, and the temperature value considered in the sensitivity analysis is that at the reactor outlet. When taking instead the reactant conversion as the independent variable, as in the x-MV criterion, we implicitly consider the possibility of complete conversion, which can only be assured in reactors of infinite length. In fact, in this case the reactor length does not appear in the model. It follows that the x-MV criterion does not account for the occurrence of the PAO region, thus providing runaway boundaries that are always more conservative than those predicted by the z-MV criterion.

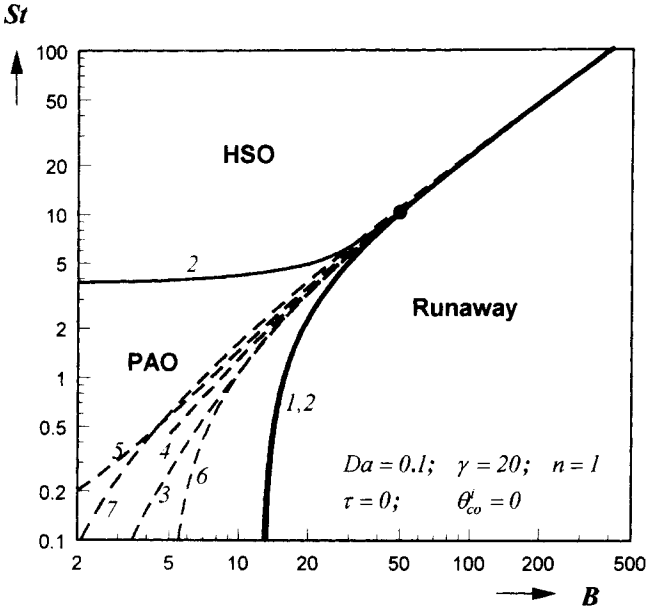

Figure 8. A comparison of the predicted runaway boundaries by various criteria in the case where the PAO occurs: 1 – z-MV; 3 – x-MV; 4 – DC; 5 – HP; 6 – AE; 7 – VF.

Curve 2 corresponds to the PAO boundary; ● indicates end of PAO region.

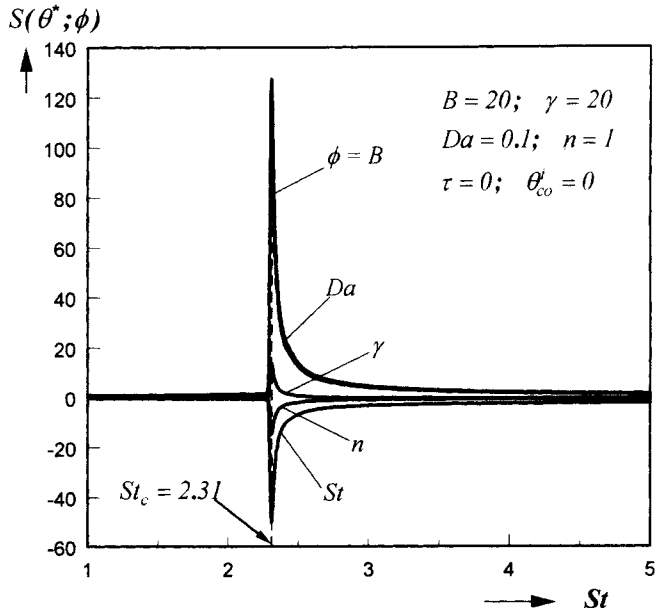

Figure 9. Normalized objective sensitivity $S(\theta^*;\phi)$ as a function of St for various choices of the parameter ϕ for the case where the axial coordinate is taken as the independent variable.

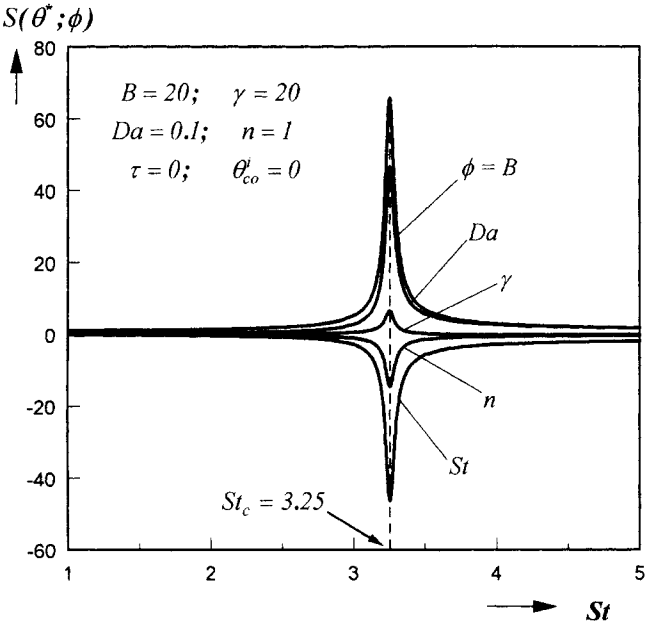

Figure 10. Normalized objective sensitivity $S(\theta^*;\phi)$ as a function of St for various choices of the parameter ϕ for the case where conversion is taken as the independent variable.

The above conclusions can be further illustrated by considering the conversion values corresponding to critical conditions for runaway, at both the temperature maximum (x_m) and the reactor outlet (x^o), reported in Table 1. For both the z-MV and x-MV criteria, the outlet values are computed by directly integrating the system Eqs. 7, 8 and 10 up to $z = 1$. For the conditions shown in Figure 3 with $Da = 0.2$ and $B = 20$, it is found that for the z-MV criterion $x_m = x^o = 0.817$, that is, the temperature maximum is located at the reactor outlet, indicating that the critical condition belongs to the PAO region. For the x-MV criterion, instead, $x_m = 0.846$, and $x^o = 0.204 < x_m$, which indicates that the temperature maximum occurs outside the given reactor, and, hence, is unrealistic. Thus, for a given reactor length, the relevant critical St value is that predicted by the z-MV criterion. However, we can retain some significance to the x-MV criterion, as with all other criteria based on the behavior in the temperature-conversion phase plane, by regarding it as a conservative estimate.

In summary, *for a reactor of given length, because of the possible existence of the PAO regime, when one uses the MV generalized criterion to predict the critical conditions for runaway, the axial coordinate of the reactor has to be used as the independent variable.*

Table 1. Critical St Values for Runaway Given by the z-MV and x-MV Criteria, Respectively, and Corresponding Conversion Values at the Temperature Maximum and Reactor Outlet x_m and x^o for the Conditions Shown in Figure 3 with $Da = 0.2$ and $B = 20$

	z-MV	x-MV
St_c	2.306	3.252
x_m	0.817	0.846
x^o	0.817	0.204

In Figure 8, the predictions given by the other criteria, that is, AE, DC, HP and VF are also shown. It is seen that, similar to the x-MV criterion, they all provide in the PAO regime exceedingly conservative predictions of the runaway boundary. In particular, the AE, DC and VF criteria (that is, curves 6, 4 and 7) are based on some geometric feature of the temperature profile along the reactor axis (DC) or reactant conversion (AE and VF). Since the obtained results are substantially equivalent, we can conclude that the conservative predictions are due to the geometric nature of these criteria, independent of whether or not the constraint on reactor length is accounted for. In fact, it can be shown through numerical calculations that for the AE and DC criteria, which are based on the first appearance of a region with positive second-order derivative before the temperature maximum, even though the temperature maximum is located outside the reactor in the case of PAO, the positive second-order derivative can occur inside the reactor. A similar behavior is also exhibited by the HP criterion (curve 5), which defines the critical condition for runaway as the first appearance of a minimum on the $s(\theta;\theta^i) - z$ profile before the temperature maximum. Note that this criterion, although using the sensitivity concept, it still a geometry-based criterion, which is different from the MV generalized criterion that is instead based on the quantity (the maximum) of the normalized objective sensitivity.

Finally, note that for large B values, as shown in Figure 8, all criteria yield essentially identical results. This is so because in such cases, runaway occurs soon after the reactor inlet at negligible reactant conversion. Thus, all criteria approach the classic criterion of Semenov.

Thus, summarizing the z-MV criterion provides the best representation of the reactor runaway behavior, and this leads to the regions of reactor operation identified by curves 1 and 2 in Figure 8. It appears that *three regimes are possible: two of them are safe and may either exhibit a temperature maximum along the reactor (HSO) or not (PAO), while the third regime corresponds to runaway and always includes a temperature maximum.*

The shape of the reactor operation regions shown in Figure 8 is typical for relatively low Da values. As the Da value increases, the PAO region shrinks and may even disappear, as shown in Figure 11, where the PAO and runaway boundaries are shown for various values of Da. This indicates that for sufficiently large Da values, the transition from HSO to runaway occurs directly, without involving the PAO region, even at relatively low values of the heat of reaction parameter B. The reason is that for large Da values, high reactant conversion occurs, leading always to a temperature maximum inside the reactor. It should also be mentioned that for relatively high Da, in the region of small B values, the system becomes intrinsically insensitive and the predicted critical boundary between safe and runaway operation has less physical meaning and accordingly the runaway criterion loses its generalized character. This leads to deviations between the PAO and the runaway boundaries which appear in Figure 11, such as in the case of $Da = 0.2$.

It is worth mentioning that in most cases in the literature, the runaway boundaries are given in the $St/(DaB) - B$ pa-

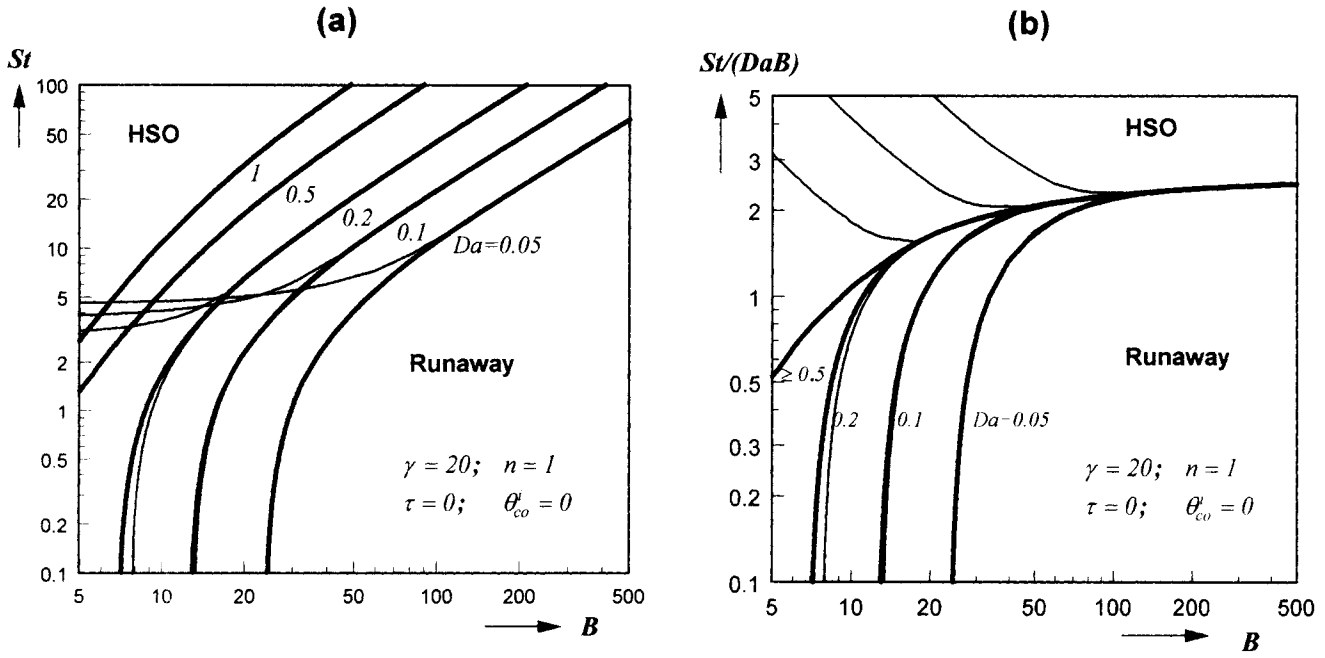

Figure 11. Runaway boundaries (thicker curves) predicted by the *z*-MV criterion for various values of *Da*, together with the PAO boundaries (thinner curves): in the (a) *St* – *B*; (b) *St/(DaB)* – *B* parameter plane.

rameter plane. When one takes the conversion as the independent variable, this is the natural choice, since as can be seen from Eq. 13, *St/(DaB)* is an independent parameter. The predicted runaway boundaries in this case are independent of *Da*. When one takes the axial coordinate as the independent variable, the results shown in Figure 11b indicate that the runaway boundaries are still independent of *Da* if the reactor operates in the HSO region, while they become a function of *Da* if the reactor operates in the PAO region.

Runaway region with varying coolant temperature

The influence of varying coolant temperature on reactor runaway behavior was first investigated by Soria Lopez et al. (1981) and later by Hosten and Froment (1986) through an extension of the VF criterion for constant external cooling. Similarly, Henning and Perez (1986) extended the HP criterion to this case, while Bauman et al. (1990) adopted the *x*-MV criterion.

Let us first compare the predictions given by the *z*-MV and the *x*-MV criteria. Figure 12 shows the computed runaway boundaries in the $St - B$ parameter plane for various τ values, where the solid and broken curves denote the results given by the *z*-MV and the *x*-MV criteria, respectively. Note that the corresponding PAO boundaries in this case coincide with the runaway boundaries given by the *z*-MV criterion.

In the case of constant external cooling shown in Figure 8, we have seen that the *z*-MV and the *x*-MV criteria give the same predictions for the runaway boundaries, when the adjacent safe reactor operation is in the HSO regime. On the other hand, when the adjacent safe region is in the PAO regime, the *x*-MV criterion gives conservative results. In the case of co-current external cooling shown in Figure 12a, it is seen that the transition from safe to runaway operation occurs always when the reactor is in the PAO regime, and, hence, the predictions of the two criteria are always rather different. Similarly to the case of constant external cooling, this behavior is due to the constraint imposed by the finite reactor length, which is accounted for by the *z*-MV criterion, but ignored by the *x*-MV criterion. This is confirmed by the observation that for all the conditions corresponding to criticality for runaway predicted by the *x*-MV criterion, the temperature maximum occurs for conversion greater than that at the reactor outlet. It is worth pointing out that the differences shown in Figure 12a are related to the specific operating conditions employed. For example, by increasing values of the reactor length and maintaining all the other parameters fixed, the results of the *x*-MV criterion approach those given by the *z*-MV criterion. In particular, by increasing the value of *St* while keeping the ratio *St/Da* constant, the critical value of the heat of reaction parameter *B* predicted by the *z*-MV criterion decreases and approaches the value given by the *x*-MV criterion, which instead remains unchanged.

A further confirmation of the conclusions above is given by the comparison between the predictions of the two criteria shown in Figure 12b, where although reduced to a small island, a region exists where safe HSO is possible. It can be seen that the critical *St* values given by the *z*-MV and the *x*-MV criteria are close and in fact coincide when the runaway boundary is close to the HSO regime. In conclusion, for reactors with cocurrent external cooling, even more than for those with constant external cooling, the use of the *z*-MV criterion is recommended.

In general, and particularly in the case of constant external cooling examined earlier, the critical conditions for runaway are reported in the $St - B$ or in the *St/DaB*(or ψ) – *B* parameter plane. Here, the boundaries between the safe and runaway behavior provide the critical wall heat-transfer rate as a function of the heat generation rate. In the case of cocurrent external cooling, the representation of the runaway

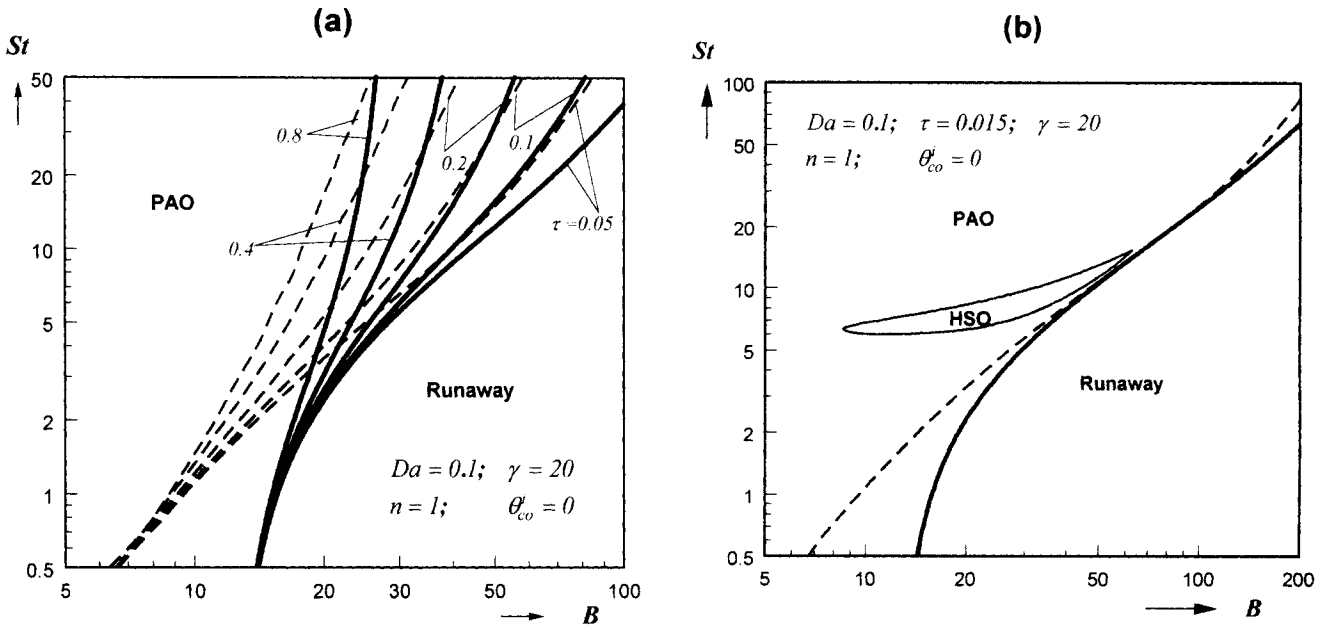

Figure 12. Runaway boundaries in the *St*-*B* parameter plane, predicted by the *z*-MV (solid curves) and the *x*-MV (broken curves) criteria for various τ values.

The solid curves correspond also to the PAO boundaries.

regions in the $\tau - B$ parameter plane with a fixed value of *St* may be more useful in practical applications. The critical value of the parameter τ indicates in fact how the heat capacity of the external coolant should be chosen in order to prevent the reactor from runaway for given heat generation and wall heat-transfer rates. Figures 13a, 13b, and 13c illustrate the runaway boundaries given by the various criteria in the $\tau - B$ parameter plane, together with the corresponding PAO boundaries for three values of *Da*. Note that the PAO boundaries in this case have two branches (one lower and one upper) with respect to *B*, which, as discussed above in the context of Figure 7 where the logarithmic scale better evidences the two branches, separate the PAO regime from two different types of HSO. The one below the lower branch (low τ values) is characterized by low reaction rates and low outlet conversion, while the HSO above the upper branch is characterized by high reaction rates and essentially complete outlet conversion. In general, we see that below the bifurcation point of the PAO boundary (curve 7), the critical conditions for runaway predicted by the various criteria are substantially identical. These are given by the curve emerging from the bifurcation point and going towards low τ values, which is actually a short curve best evidenced in Figure 13c. However, in the region above the bifurcation point of the PAO boundary, the critical conditions given by all criteria are rather different. These results are similar to those discussed for reactors with constant external cooling, with reference to the $St - B$ parameter plane, shown in Figure 8. In particular, we see again that when the transition from safe to runaway operation occurs with the reactor operating in the HSO (safe) regime, all criteria are substantially in agreement. On the other hand, if the reactor is in the PAO regime, then different criteria provide different predictions of the critical conditions for runaway.

Moreover, in Figure 13a, above the bifurcation point of the PAO boundary, the runaway boundary predicted by the *z*-MV criterion (curve 1) coincides with the upper branch of the PAO boundary, while those given by all the other criteria are located inside the PAO region, indicating exceedingly conservative conditions.

As the *Da* value increases as shown in Figures 13b and 13c, the PAO and all the predicted runaway boundaries move towards lower *B* values, where the runaway phenomenon becomes intrinsically less intensive. As a result, the runaway boundaries given by the various criteria become less reliable. In Figure 13c, the runaway boundary predicted by *z*-MV criterion (curve 1) also tends to deviate from the PAO boundary (curve 7) and to move inside the PAO region. Moreover, for large values of τ in Figure 13c, the critical *B* values predicted by *z*-MV criterion become smaller than those predicted by the *x*-MV, that is, more conservative.

In order to better understand the last phenomenon observed above, let us consider the runaway boundaries predicted by both the *x*-MV and *z*-MV criteria for a further increased *Da* value ($Da = 0.4$), as shown in Figure 14a. It is found that in this case, the *z*-MV criterion predicts *two* independent runaway boundaries (curves 1): one located in the PAO region, and another in the HSO region which coincides with that predicted by the *x*-MV criterion (curve 2). The development of the double runaway boundaries for the *z*-MV criterion can be understood from Figure 14b, where the profiles of the normalized objective sensitivity $S(\theta^*; B)$ as a function of *B* are shown for various values of τ. For the given set of parameters in Figure 14a, it can be shown from Figure 11 that at $\tau = 0$ the reactor operates in the HSO region for any given value of *B*, and, hence, the temperature maximum θ^* for defining the normalized objective sensitivity $S(\theta^*; B)$ for both the *z*-MV and the *x*-MV criteria, is the same. Thus,

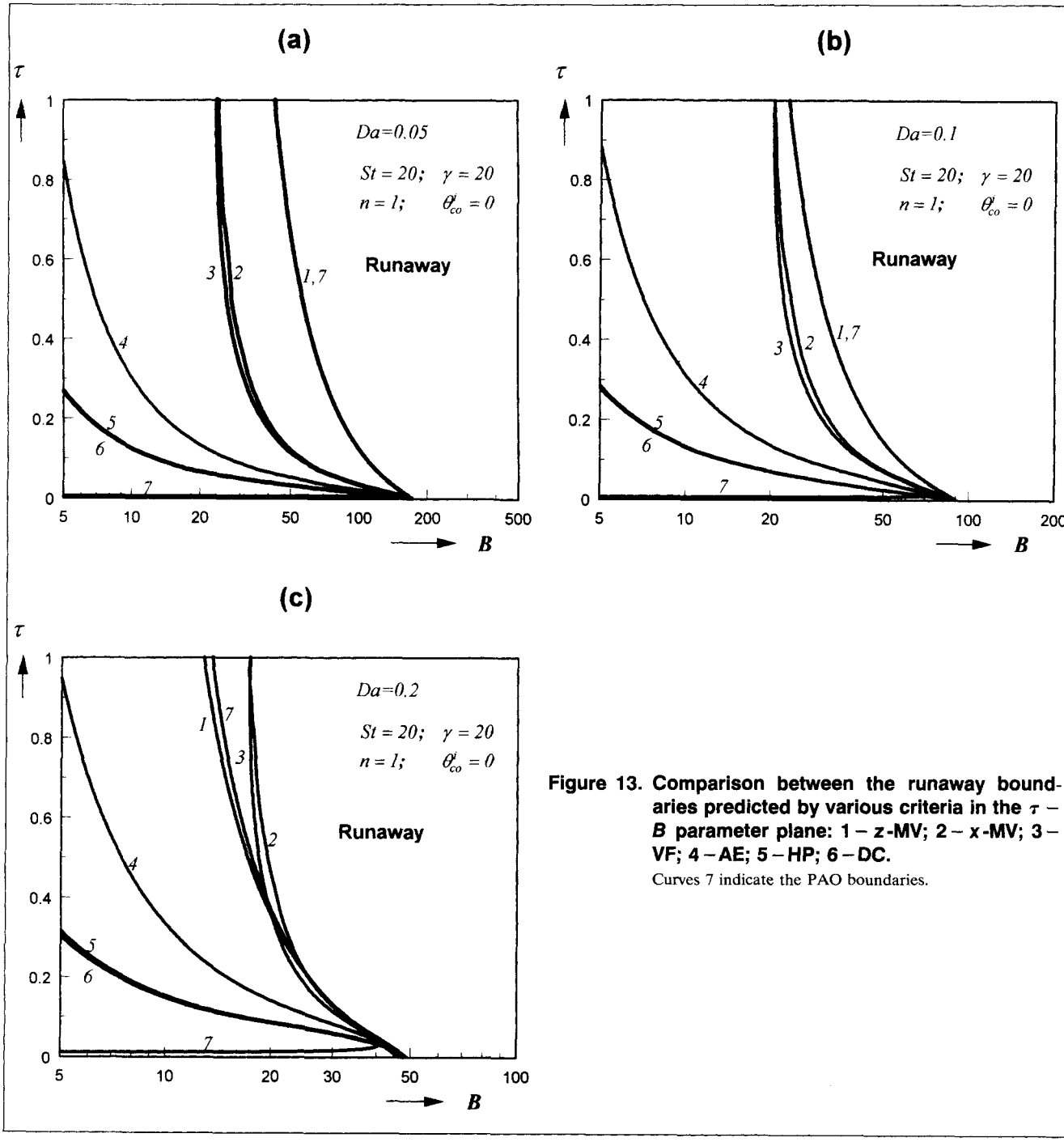

Figure 13. Comparison between the runaway boundaries predicted by various criteria in the $\tau - B$ parameter plane: 1 – z-MV; 2 – x-MV; 3 – VF; 4 – AE; 5 – HP; 6 – DC.

Curves 7 indicate the PAO boundaries.

the $S(\theta^*; B)$ profile for $\tau = 0$ in Figure 14b is the same for both the z-MV and the x-MV criteria, and the sharp sensitivity peak gives the critical B value for runaway. As τ increases, the PAO appears in the region of low B values. Now, if for each τ value we compute the $S(\theta^*; B) - B$ profile for B values greater than that corresponding to the PAO boundary, the sensitivity profiles for both the z-MV and the x-MV criteria remain still the same, and yield the second peak in the case of $\tau = 0.1$, 0.6, or 1 shown in Figure 14b. As a result, we obtain a merged runaway boundary (the solid curve 1,2) that is located in the HSO region in Figure 14a. On the other hand, if we compute the $S(\theta^*; B) - B$ profile inside the PAO region for the z-MV criterion, we obtain another peak for each τ value. This corresponds to the first peak in the case of $\tau = 0.1$, 0.6, or 1 shown in Figure 14b, which arises from the sensitivity behavior of the reactor outlet temperature. This leads to the broken curve 1 located inside the PAO region in Figure 14a. Since the temperature maximum at the reactor outlet cannot be identified by the reactor model with conversion as the independent variable, the broken curve in Figure 14a is not found using the x-MV criterion.

When two peaks in the $S(\theta^*; B) - B$ curve exist, the first one which arises in the PAO region and occurs at low B values is generally of low magnitude. On the other hand, the

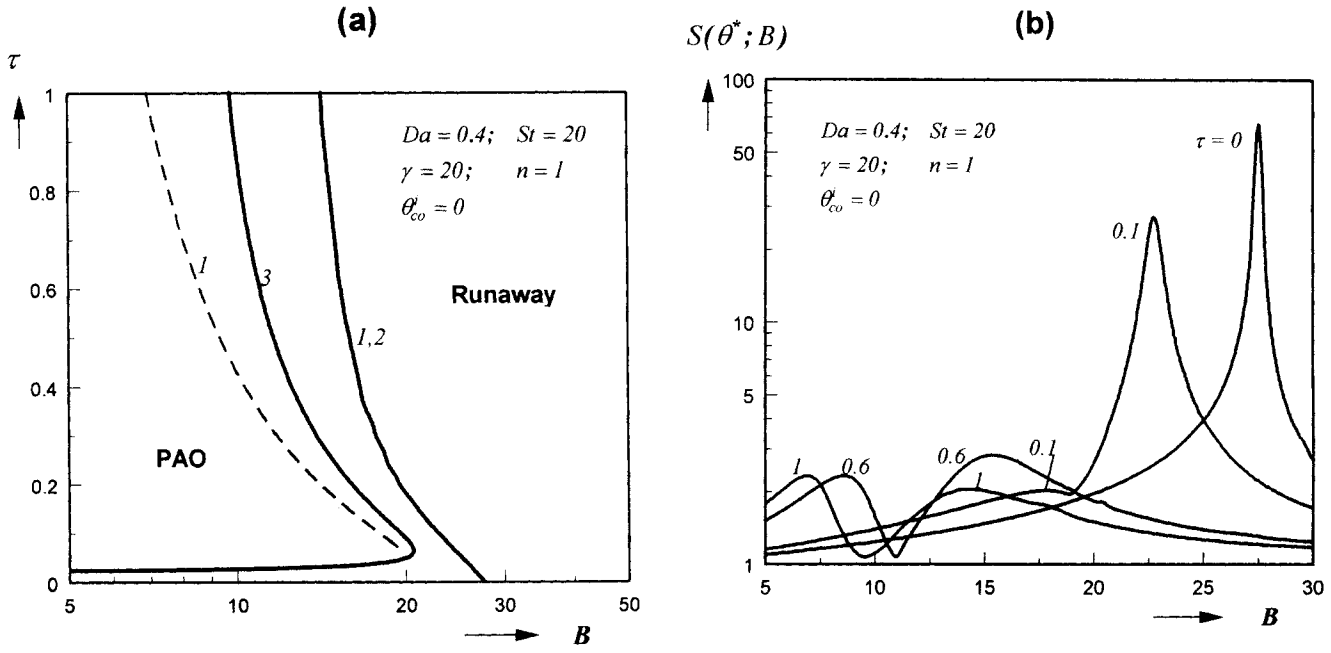

Figure 14. (a) Runaway boundaries predicted by z-MV (curves 1) and x-MV (curve 2) criteria and PAO boundary (curve 3) in the τ-B plane; (b) values of the normalized objective sensitivity $S(\theta^*; B)$ as a function of B for various values of τ in (a).

$Da = 0.4$; all the other parameters as given in Figure 13.

second peak in the HSO region is sharper, indicating significant sensitive behavior. Thus, the second peak is the true indicator of runaway behavior. It should also be mentioned that for the runaway boundary in the case of high τ and Da values, where the critical B value is low, the reactor operates in a parametrically insensitive region, characterized by relatively low values of the sensitivity maximum, as shown in Figure 14b. In such cases, one cannot define a generalized boundary indicating a transition between runaway and safe operations.

Conclusions

For tubular reactors with either constant or varying external cooling, the reliability of various runaway criteria reported in the literature has been assessed through a comparison between the critical runaway conditions predicted by these criteria and the generalized one (Morbidelli and Varma, 1988) using axial coordinate as the independent variable. It is found that all criteria predict substantially the same critical conditions when a hot spot is present inside the reactor, that is, the reactor operates in the HSO region. When the hot spot shifts to the reactor outlet, that is, the reactor operates in the PAO region, however, the critical conditions predicted by all criteria deviate from one another.

When the reactor operates in the PAO region, the best representation of the critical conditions for runaway is given by the generalized criterion using reactor axial coordinate as the independent variable, and the computed runaway boundary coincides with the PAO boundary. All the criteria based on the geometric feature of reactor temperature profiles give exceedingly conservative predictions, and the runaway boundaries are located inside the PAO region. *Thus, the generalized criterion is recommended for predicting the critical conditions for runaway in tubular reactors with either constant or varying external cooling.*

In the PAO region, also, the generalized criterion can give conservative predictions if reactant conversion is used as the independent variable in the reactor model. This arises because, in this case, the effect of the reactor length on the temperature behavior is ignored and in the definition of the normalized objective sensitivity, unrealistic temperature maxima that might occur only outside the reactor are used. *Therefore, for a reactor of given length, because of the possible existence of a PAO regime, when the MV generalized criterion is used to predict the critical conditions for runaway, the axial coordinate of the reactor should be used as the independent variable in the reactor model.*

Notation

c_p = mean specific heat of reactant mixture, J/(K·kg)
$c_{p,co}$ = mean specific heat of coolant, J/(K·kg)
C = reactant concentration, mol/m^3
d_t = reactor diameter, m
E = activation energy, J/mol
ΔH = heat of reaction, J/mol
f_i = (i = 1, 2) functions, defined by Eqs. 7 and 8
k = reaction rate constant, (mol/m^3)$^{1-n}$/s
l = axial coordinate of the reactor, m
L = reactor length, m
ρ = density of the fluid mixture, kg/m^3
ρ_B = bulk density of the reactor bed, kg/m^3
R_g = ideal gas constant, J/(K·mol)
$s(y; \phi) = (\partial y/\partial \phi)$ local sensitivity of the output variable y to the input parameter ϕ
St = Stanton number, defined by Eq. 6
t_n = number of reactor tubes
T = temperature, K

U = overall heat-transfer coefficient, J/(m^2·s·K)
v^o = superficial velocity, m/s
x = reactant conversion, defined by Eq. 5
$z = l/L$

Superscripts

i = reactor inlet
o = reactor outlet

Subscripts

c = critical condition
co = coolant

Literature Cited

Adler, J., and J. W. Enig, "The Critical Conditions in Thermal Explosion Theory with Reactant Consumption," *Comb. Flame*, **8**, 97 (1964).

Barkelew, C. H., "Stability of Chemical Reactors," *Chem. Eng. Prog. Symp. Ser.*, **25**, 37 (1959).

Bauman, E., A. Varma, J. Lorusso, M. Dente, and M. Morbidelli, "Parametric Sensitivity in Tubular Reactors with Co-current External Cooling," *Chem. Eng. Sci.*, **45**, 1301 (1990).

Dente, M., and A. Collina, "Il Comportamento dei Reattori Chimici a Flusso Longitudinale nei Riguardi della Sensitività," *Chim. e Industria*, **46**, 752 (1964).

Hagan, P. S., M. Herskowitz, and C. Pirkle, "Runaway in Highly Sensitive Tubular Reactors," *SIAM J. Appl. Math.*, **48**, 1437 (1988).

Henning, G. P., and G. A. Perez, "Parametric Sensitivity in Fixed-Bed Catalytic Reactors," *Chem. Eng. Sci.*, **41**, 83 (1986).

Hlavacek, V., M. Marek, and T. M. John, "Modeling of Chemical Reactors: XII," *Coll. Czech. Chem. Comm.*, **34**, 3868 (1969).

Hosten, L. H., and G. F. Froment, "Parametric Sensitivity in Co-current Cooled Tubular Reactors," *Chem. Eng. Sci.*, **41**, 1073 (1986).

Morbidelli, M., and A. Varma, "Parametric Sensitivity and Runaway in Tubular Reactors," *AIChE J.*, **28**, 705 (1982).

Morbidelli, M., and A. Varma, "On Parametric Sensitivity and Runaway Criteria of Pseudohomogeneous Tubular Reactors," *Chem. Eng. Sci.*, **40**, 2165 (1985).

Morbidelli, M., and A. Varma, "A Generalized Criterion for Parametric Sensitivity: Application to Thermal Explosion Theory," *Chem. Eng. Sci.*, **43**, 91 (1988).

Soria Lopez, A., H. de Lasa, and J. A. Porras, "Parametric Sensitivity of a Fixed Bed Catalytic Reactor. Cooling Fluid Flow Influence," *Chem. Eng. Sci.*, **36**, 285 (1981).

Thomas, P. H., "Effect of Reactant Consumption on the Induction Period and Critical Condition for a Thermal Explosion," *Proc. R. Soc.*, **A262**, 192 (1961).

van Welsenaere, R. J., and G. F. Froment, "Parametric Sensitivity and Runaway in Fixed Bed Catalytic Reactors," *Chem. Eng. Sci.*, **25**, 1503 (1970).

Manuscript received May 29, 1997, and revision received Feb. 2, 1998.